Electrically conductive and super-tough polyamide-based nanocomposites

Aravind Dasari[a,b], Zhong-Zhen Yu[c] and Yiu-Wing Mai[a]

[a] *Centre for Advanced Materials Technology (CAMT), School of Aerospace, Mechanical and Mechatronic Engineering J07, The University of Sydney, Sydney, NSW 2006, Australia*

[b] *Madrid Institute for Advanced Studies of Materials (IMDEA-Materials), E. T. S. de Ingenieros de Caminos, 28040 Madrid, Spain*

[c] *Department of Polymer Engineering, College of Materials Science and Engineering, Beijing University of Chemical Technology, Beijing 100029, China*

Abstract

Polymer nanocomposites can exhibit superior multi-functional properties if they possess phase separated morphology at the nanoscale. Despite the huge potential of these materials, there are several fundamental issues including the ultimate microstructures, which need to be resolved to tailor different physical and mechanical properties required for specific applications. A 'ternary nanocomposites' approach is adopted to prepare electrically conductive and super-tough^ (in terms of notched impact energy) hybrid polymer nanocomposites (polyamide 6/carbon nanotube /elastomer) that possesses better properties than either of the constituent binary polymer nanocomposites (polyamide 6/carbon nanotubes and polyamide 6/elastomer). The individual roles of the nano-fillers involved in achieving multi-functionality are emphasized. The level of property enhancements of ternary nanocomposites depends essentially on the microstructure inducing a volume-exclusion effect and the capability of fillers to activate the plastic deformation mechanisms in the matrix.

Keywords: Carbon nanotubes, Nanocomposites, polyamide, Conductivity; Toughness

---

^ Super-tough means notched impact energy larger than 50 kJ/m^2 using a standard Izod test

1. Introduction

In the last two decades, nanostructured materials like polymer nanocomposites have gained significant interests in both fundamental and applied research because of the exceptionally large surface area-to-volume ratio of the nano-additives available for interaction with the polymer matrix. Exploitation of this and other characteristics of nanoscale fillers results in the attainment of multi-functional (that is, unique combinations of mechanical, physical, optical, electrical and thermal) properties required for a spectrum of applications [1-4]. Carbon nanotubes (CNTs) are a good representative example of the multi-functional nano-fillers. They have exceptional elastic modulus, strength, aspect ratio, electrical and thermal conductivity, and chemical stability. Their potential, however, has not been fully realized after their incorporation into polymers and the properties of the nanocomposites obtained are often below par of the predicted values [5-9]. In addition, there are many discrepancies and uncertainties in the literature, particularly on their mechanical properties. Most studies have reported improvements in stiffness and strength; but toughness results are rather mixed. Even large variations in the percolation threshold of polymer /CNT materials are noted. Despite the debates on the magnitudes of enhancements/reductions of mechanical properties or the variations in percolation threshold, they are being used in many applications, ranging from structural to biomedical. For example, polymer/CNT nanocomposites are being actively used in aerospace applications requiring electrical conductivity for dissipating electrostatic charges and electromagnetic interference shielding [3]. Even the high dielectric permittivities of these materials are exploited to use them as actuators for artificial muscles since they can change their shape in response to an applied external electric field [10].

A critical issue in taking advantage of the superior properties of CNTs is the ability to disaggregate and control their dispersion in the polymer. This is due to the existence of entangled/intertwined networks and the high intermolecular van der Waals interactions among the CNTs. There are several methods to incorporate them into polymers including *in situ* polymerization, film casting of suspensions of nanotubes in dissolved polymers, and melt compounding [5-9, 11-15]. Ball milling, high energy sonication and high speed stirring are used conjointly with the above methods to achieve optimum physical blending. Another strategy is to use functionalized CNTs (e.g., oxidation or grafting). As the surface area of nanotubes is important for interfacing with the polymer and stress transfer, it is also necessary to consider the differences between single- and multi-walled nanotubes [16, 17]. Single-walled nanotubes provide a maximum specific surface area when compared to multi-walled nanotubes; however, the former experiences strong attractive forces amongst themselves resulting in agglomeration. Despite a larger diameter (owing to several concentric walls) and relatively smaller interface for stress transfer, multi-walled nanotubes exhibit better dispersion.

Thostenson and Chou [11] reported significant improvements in toughness of epoxy at relatively low loadings (<2 wt%) of multi-walled CNTs and attributed this to the increase in roughness of

the fracture surfaces and nanotube pull-out from the matrix. Satapathy *et al.* [13] investigated the fracture behavior of double-edge-notched tensile samples and, based on their SEM observations, reported bridging by CNTs across the crack-tip and underneath the advancing crack (transverse to the tensile direction) as the major toughening mechanism in polycarbonate/CNT (2 wt%) nanocomposite. Similarly, in poly(methylmethacrylate)/multi-walled CNT composites, Gorga and Cohen [18] suggested that the orientation of nanotubes is necessary for toughness improvements. With 1 wt% nanotubes, a drastic increase in toughness was obtained and attributed to crack-wake bridging (when the nanotubes are oriented normal to the craze/crack growth direction). Ma *et al.* [19] reported the effect of silane grafted multi-walled nanotubes on fracture toughness; they noted a decrease of K_{IC} for untreated nanotubes/epoxy composite and a moderate increase in silane-CNT/epoxy nanocomposites (up to 0.5 wt% loading). These differences were explained in terms of the dispersion and interfacial interactions between CNT and epoxy and identified the toughening mechanisms as crack pinning and crack tip bifurcation.

As discussed in the few examples above and in many other studies reported in the literature, the increase in toughness of polymer/CNT nanocomposites was mainly caused by the nanotube pull-out mechanism and their bridging of cracks in the matrix. The pull-out mechanism inspired from conventional polymer/fiber composites, where fiber/matrix debonding and fiber pull-out (including work done against sliding friction in pulling out the fiber) govern the extent of energy absorption. With this concept, the very high interfacial areas in polymer/nanotube composites are expected to result in drastic improvements in work of fracture due to nanotube pull-out. Wagner and co-workers [20-22] studied the pull-out concept on individual nanotubes by attaching them to the end of a scanning probe microscope (SPM) tip and pushing into the liquid epoxy polymer (or liquid melt of polyethylene-butene). After the polymer had solidified the nanotube was pulled out and the forces were recorded from the deflection of the SPM tip cantilever. Although this provided an idea of the interfacial strength of individual nanotubes, it is not directly relevant to pull-out toughness measurements as it depends on many factors. For example, by increasing the nanotube embedded length in the resin, the nanotube breaks instead of being pulled out from the polymer. Even the alignment/orientation and flexible/entanglement nature of the nanotubes are critical and affect the pull-out of nanotubes making it difficult for comparison between the two concepts (that is, conventional pull-out *versus* pull-out of individual nanotubes using SPM tip)

Very recently, based on the scaling argument [23] by correlating the radius (r), fiber strength (σ) and interface strength (τ) with the energy absorbed per unit cross-sectional area by fiber pull-out (i.e., $G_{pull\text{-}out} \sim r\sigma^2/\tau$), it was shown that the improvements in toughness in polymer/CNT nanocomposites cannot be attributed to nanotube pull-out mechanism as the pull-out energy significantly decreases when the fiber radius is scaled down to nanoscale. Wichmann, Schulte and Wagner [24] argued that this conventional correlation is not valid for nanotubes by simply considering the Kelly-Tyson expression (critical length, $l_c = r\sigma/\tau$), that is, it is impossible to vary independently the fiber radius without changing other parameters. They further suggested that if

spatial or only local bonding exists between nanotubes and matrix, this results in partial debonding of the interface and allows for crack bridging similar to conventional polymer/fiber composites as shown and analyzed by Gao *et al.* [25] two decades ago.

Nevertheless, in line with the scaling argument, there are many studies that reported reductions in toughness with the incorporation of CNTs, even at low loadings, for example, see [26, 27]. Furthermore, even with other nanoscale fillers, it is realized that conventional toughening mechanisms cannot be transferred to polymer nanocomposites directly. Johnson *et al.* [28] studied the toughening mechanisms in epoxy reinforced with ~20 nm silica particles and suggested that the conventional toughening mechanisms like crack pinning and crack deflection did not occur. In polymer/clay nanocomposites, it was shown that the individual clay layers were too small to provide toughening via mechanisms like crack bridging, deflection and pinning [29].

It is these apparent contradictions that often resulted in misleading impressions on polymer/CNT nanocomposites. Very often, poor characterization of these materials is one main reason for this confusion. Hence, one objective of the present study is to obtain a fundamental understanding of these materials by detailing their structure-property relations and fracture mechanisms using microscopy techniques. Further, the potential of CNTs to achieve multi-functional properties in the final materials is exploited by adopting a 'ternary nanocomposites' approach (which is adding dispersed soft elastomer particles to the binary polymer nanocomposites). The purpose of this is two-fold: (a) to improve the toughness and (b) to gain from the volume exclusion effect and thereby enhance the electrical conductivity. Though this is the best known approach to-date to counteract the embrittlement of polymer nanocomposites [30], its associated disadvantages must also be realized. The final microstructures are generally complex and the location of the rigid fillers (in matrix and/or rubber particles) is important in achieving the enhanced properties.

2. Experimental work

2.1. Preparation of materials

Polyamide 6 (trade name of Ultramid B3S) was obtained from BASF via Marplex Australia Pty. Ltd. A masterbatch of 20 wt% multi-walled CNTs in polyamide 6 (in the form of pellets) was obtained from Hyperion Catalysis International, USA. According to the reports from Hyperion [31], the nanotubes were vapor-grown, consist of 8-15 graphite layers wrapped around a hollow 5 nm core, and their lengths range between 1 and 10 μm. Their density is ~1.75 g/cm^3 and surface area as determined by BET (after Stephen Brunauer, Paul Emmett and Edward Teller) method is ~250 m^2/g. The masterbatch was diluted with polyamide 6 to obtain polyamide 6/CNT nanocomposites with different loadings of CNT (2.5, 5 and 10 wt%).

Polyethylene-octene copolymer grafted with 0.6 wt% of maleic anhydride (POE-g-MA) was purchased from Rui-Sheng Co. (Taiwan) and used as a toughening agent for the polyamide 6

nanocomposites. All the nanocomposites and blends were prepared by melt-compounding in a Werner & Pfeiderer ZSK-30 twin-screw extruder (L/D = 30, L = 0.88 m), followed by injection molding with a Boy Dipronic 22S injection molding machine. The extruder was operated at a temperature range of 210-245 ^{o}C and a screw speed of 300 rpm. The injection molding machine was set with the barrel and mold temperatures at 235 ^{o}C and 60 ^{o}C, respectively. All ingredients and pelletized extrudates were oven-dried at 85 ^{o}C overnight prior to melt compounding and injection molding. All the desired ingredients were blended simultaneously to fabricate the ternary nanocomposites.

2.2. Morphology observations

To study the microstructures of all the nanocomposites/blends, ultra-thin sections in the range of 60-90 nm in thickness were cryogenically cut (from the core along a plane normal to injection-molding direction) with a diamond knife at -80 ^{o}C using a Leica Ultracut S microtome with a cutting speed of 0.2 mm/s. Sections were collected using a droplet of 2.3 mol sucrose and placed on formvar/carbon coated 400-mesh copper grids. Subsequently, they were thoroughly rinsed with distilled water for at least 30 minutes to wash away the sucrose. For the POE-g-MA containing materials, sections were then carefully stained with an aqueous solution of phosphotungstic acid ($H_3PO_4.12WO_3$) and benzyl alcohol ($C_6H_5CH_2OH$) for 3-5 minutes to enhance the phase contrast between polyamide and the POE-g-MA particles. The thin sections were observed using a Philips CM12 transmission electron microscope (TEM) at an accelerating voltage of 120 kV.

2.3. Mechanical property measurements

Young's moduli and tensile strengths were measured on dumbbell shaped samples using an Instron 5567 testing machine at a crosshead speed of 50 mm/min according to ASTM Standard D638. Storage moduli and tan δ were determined using a dynamic mechanical analyzer (TA Instruments) in a single cantilever mode from –50 to +150 ^{o}C at a heating rate of 10 ^{o}C/min and a frequency of 1.0 Hz. The notched impact energy (kJ/m^2) was evaluated in an ITR-2000 instrumented impact tester according to ASTM D256 on the injection molded rectangular bars machined with a 45° V-notch (depth of 2.54 mm). All these tests were conducted at ambient temperature (20-25 °C) and an average value of 5 repeated tests was taken for each composition.

2.4. Electrical conductivity

Alternate current (AC) electrical conductivities of the materials were measured using a HP 4194A impedance analyzer at ambient temperature and frequency range from 10^2 to 10^6 Hz. Silver paste was used to ensure good contact between samples and electrodes. The dimensions of the samples were 10x10x1 mm^3.

2.5. Fracture mechanisms

The deformation and fracture mechanisms were studied by examining the fracture surface via scanning electron microscopy (Philips S-505 SEM was used) and subsurface with TEM. Post-mortem TEM analysis in a plane normal to the fracture surface near the notch tip (Scheme 1) was conducted on notched impact fractured specimens to identify the deformation history that finally led to failure.

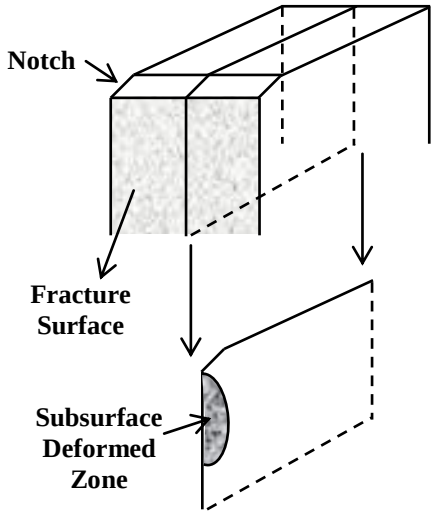

Scheme 1. Illustration of subsurface deformed zone in a plane normal to the fracture surface near the notch tip where the post-mortem TEM analysis is conducted.

3. Results and Discussion

3.1. Microstructure and mechanical properties

The dispersion, distribution and location of CNTs (5 wt% loading) in polyamide 6 matrix and in polyamide 6/POE-g-MA (75/20) blend are shown in **Figure 1**. It is evident from Figure 1a that the nanotubes are disentangled, homogeneously dispersed, and randomly oriented in polyamide matrix. However, they are close to each other and appear to form interconnecting and network-like structures due to the large aspect ratios and high loading. The diameters of the nanotubes are in the range of ~10-15 nm. As expected, based on our previous work on polyamide 6/POE-g-MA binary blends [32], POE-g-MA elastomer particles were well dispersed in the matrix at 20 wt% POE-g-MA, and so the TEM micrograph is not shown here. The dispersion of POE-g-MA rubber particles is possible owing to the *in situ* formation of a grafted copolymer generated from the reaction of the grafted maleic anhydride with the amine end groups of polyamide 6 during melt processing and thereby resulting in strong interfacial interaction between them. Size distribution analysis of POE-g-MA particles was performed by 'Image J' (National Institutes of Health, USA), which revealed a broad range of size distribution (see below).

Even in the ternary nanocomposite, majority portion of nanotubes are selectively embedded only in the continuous polyamide 6 matrix and are present to a minimum extent or absent in the POE-g-MA (see Figures 1b and 1c). In our previous investigations on polymer/rubber/clay ternary nanocomposites [32-34], it was shown that the presence of clay layers in the elastomer particles is influenced by: (a) the nature and polarity of elastomer particles (relative to clay and matrix) and (b) the blending protocol. We have further indicated that this type of microstructure, that is, absence of rigid particles in the soft elastomer phase and their complete presence in the continuous matrix is the best microstructure for toughness and stiffness. This is because the presence of clay in elastomer particles made the latter more rigid, reduced its cavitation ability and ultimately lowered the toughening efficiency; while the maximum presence of clay in the continuous matrix improved the stiffness and strength of the nanocomposite [33]. The same holds true even for polyamide 6/CNT/POE-g-MA; the remarkable toughening efficiency of POE-g-MA is not reduced even in the presence of 5 wt% nanotubes and showed a super-tough nature (given by notched Izod impact energy) of the ternary nanocomposites (Figure 2a). At a higher nanotube loading of 10 wt%, there seems to be a slight drop in impact energy, but still exhibits a tough behavior. The slight improvement in impact energy of ternary nanocomposites at 2.5 and 5 wt% loading of nanotubes compared to binary blend may be caused by an effect of POE-g-MA particle sizes due to the additional presence of nanotubes and ***not*** an effect of the nanotubes themselves contributing to the toughening mechanisms (as no mechanisms are identified that are associated with nanotubes during failure of ternary nanocomposites, see Section 3.3).

By comparing the size distributions of POE-g-MA particles (Figure 2b), it is clear that nanotubes prevented coalescence of the dispersed domains, resulting in generally reduced dispersed rubber particle sizes in the ternary nanocomposites (e.g., at 5 wt% CNT loading) compared to the binary polyamide 6/POE-g-MA blend. It is interesting to note that mixed observations were reported in polymer/rubber/organoclay nanocomposites [35-37]. If maleic anhydride modified rubbers were used, interaction between the organic modification of clay (hydroxyethyl groups) dissolved in matrix and the maleic anhydride modification of elastomer particles hindered the compatibilizing effect of the latter and increased their sizes. However, without maleic anhydride modification, clay layers restricted the coalescence of rubber particles and thereby reduced their sizes. This suggests that while using maleic anhydride modification is important for compatibilization with the polyamide matrix, it also has a negative effect when blended with organoclay resulting in increased rubber particle size. In contrast, if compatibility between matrix and rubber particles is poor, this may lead to a poor interface and interfacial debonding of the rubber particle from the matrix under loading rather than cavitation, which will affect the toughening mechanisms and the toughness value. Nevertheless, no such phenomenon is observed here with the CNT and the compatibility between POE-g-MA and polyamide is expected to be good.

But the main drawback of this approach of incorporating elastomer particles in the binary nanocomposites is the requirement of a substantial elastomer concentration (usually >15 wt%). Even in the current study, 20 wt% elastomeric loading is used to achieve super-tough status. The usage of such a large amount of soft phase has a compromising effect on elastic modulus and strength; albeit elastic moduli/strength properties of the ternary nanocomposites are higher than the binary blend, they are still far below those of the neat polymer (Figure 2c). Figure 3 shows the storage moduli of neat polyamide 6, polyamide 6/POE-g-MA binary blend, and polyamide 6/POE-g-MA/CNT ternary nanocomposites as a function of temperature. Even a similar effect of reduced (storage) modulus in the presence of 20 wt% soft POE-g-MA is evident when compared to neat polymer, particularly at temperatures below their T_g. Further, the addition of nanotubes also yielded reduced damping (reduced tan δ peak height) of the polyamide matrix (not shown here). The reduced peak height is a direct result of the volume exclusion effect since the carbon nanotubes are effectively located in the matrix and absent in the elastomeric phase (20 wt%).

3.2. Electrical conductivity

Figure 4a shows the dependence of AC conductivity on the nanotube loading at a selected frequency of 10^3 Hz. As is expected, conductivity increased with increasing nanotube loading and an electrical percolation threshold is seen between 2.5 and 5 wt% in the polyamide 6/POE-g-MA materials. This indicates that from and above 5 wt% CNT loading, a continuous conductive network forms in the nanocomposites permitting a higher percentage of electrons to flow through the samples. Interestingly, conductivities of ternary nanocomposites are higher than the binary nanocomposites at similar CNT content indicating the effect of volume exclusion (see below). The frequency dependence of AC electrical conductivity of all materials in the frequency range 10^2-10^6 Hz is shown in Figure 4b, which indicates the overall connectivity of the conducting network. Even here the differences in ternary and binary nanocomposites at similar CNT loading are distinct, indicating the multi-functionality of ternary nanocomposites. Above the percolation threshold, it is expected that the ohmic conduction pathway would be active and result in the invariability of AC conductivity over the entire frequency range. From Figure 4b, however, it can be seen that the conductivity values increases with frequency suggesting some dielectric loss.

With the incorporation of POE-g-MA, the volume of polyamide 6 available for CNTs to occupy decreases, and hence results in a greater concentration of ‘conductive’ elements within the continuous polyamide matrix. Because of this “volume-exclusion” effect [38-41], the electrical conductivities are higher in the ternary nanocomposites than their corresponding binary nanocomposites. This effect of immiscible blends on conductivity was also observed in many other systems including high density polyethylene (HDPE)/polypropylene/carbon black (CB) [38], HDPE/ultra-high molecular weight polyethylene (UHMWPE)/CB [39], HDPE/ polyvinylidene fluoride/CB [40], and so forth. Owing to the melt viscosity differences between the blends in these systems, the CB particles were predominantly located in the HDPE phase of the blend. Similarly, in a ternary composite consisting of UHMWPE, low molecular weight

polyethylene (LMWPE) and CB particles, the CB particles are selectively dispersed in the LMWPE phase only [41]. This localization of CB particles resulted in a much lower percolation threshold than that exhibited by either of the constituent polymers. However, this localization of CB particles within one phase of an immiscible blend depends on both the CB loading and the blend composition.

Despite the excellent dispersion of nanotubes in the present study, the percolation threshold is rather high compared to other systems reported in the literature. Even ultra-low percolation thresholds in the range of 0.0021-0.0039 wt% [42] and 0.0052-0.0085 vol% [43] for epoxy/CNT nanocomposites were reported. Major uncertainties are with the type and quality of nanotubes, that is, a wide variety of synthesis methods have been employed to obtain nanotubes of different sizes, aspect ratios, crystalline orientation, purity, entanglement, and straightness. It was reported that when the aspect ratio of CNTs was reduced from 417 to 83 and 8.3 in epoxy/CNT nanocomposites, the corresponding percolation threshold increased from 0.5 to 1.5 and > 4 wt%, respectively, indicating that the aspect ratio is a predominant factor [44]. On the contrary, for an aspect ratio of 300, Kim *et al.* [45] reported a percolation threshold of 0.017-0.077 vol% in epoxy/CNT nanocomposites; while even with an aspect ratio of 1000, Allaoui *et al.* [46] obtained a percolation threshold at 0.6 vol%. In another recent study, it was reported that depending on the processing technique used to prepare epoxy/multi-walled CNT nanocomposites, dispersion states and CNT aspect ratios varied and a combination of these two parameters affected the percolation threshold [47].

Nevertheless, it is rather interesting to note that even with the same kind of Hyperion nanotubes [31], percolation threshold varied depending on the matrix materials. Potschke *et al*. [48] have reported an electrical threshold between 1 and 2 wt% with polycarbonate as matrix despite the apparent diameter of tubes varied from 10 to 50 nm suggesting an adsorbed layer of polymer on the tubes. With polyvinyl alcohol as matrix and same Hyperion nanotubes as fillers, Shaffer and Windle [49] reported a percolation threshold between 5 and 10 wt% of nanotubes. Sandler *et al.* [50] also reported a percolation threshold between 0.0225 and 0.04 wt% in epoxy nanocomposites based on these nanotubes. In yet another study on polycarbonate nanocomposites, electrical resistivity measurements indicated that the percolation of nanotubes has reached between 1 and 1.5 wt% [51]. Although differences in melt viscosity and percentage crystallinity may qualitatively explain the observed variations in the percolation threshold with different matrices, proper experimental evidences are still lacking.

3.3. *Fracture mechanisms*

The impact fracture surfaces of neat polyamide 6 (Figure 5a) and polyamide 6/CNT binary nanocomposite (Figure 5b) are very similar and show a typical brittle morphology with hackles (occupying the majority of fracture area) emanating radially from the primary crack initiation site (small smooth region identified by a white arrow). Close examination of Figure 5b indicates

that upon fracture most of the nanotubes are broken with the other ends still strongly embedded in the matrix (represented as white dots in Figure 5c). There is little indication of formation of cavities from debonding or pull-out of nanotubes in the binary nanocomposite. Due to the inherent brittleness of the samples, small chips of material may be removed during the fast fracture process which may give the appearance of voids (as indicated by the white arrows). Nevertheless, to accurately identify the fracture processes involved, postmortem TEM analysis in a plane transverse to the fracture surface near the notch tip (distance up to ~500 μm from fracture plane) was also conducted. But no noticeable deformation features are observed even close to the notch tip, except for slight alignment/orientation of the nanotubes (Figure 5d) along the plastic flow direction. This indicates strong interfacial adhesion between nanotubes and matrix. Without any mechanisms to relieve the constraint imposed by the nano-reinforcement, polyamide 6 matrix fractures in a brittle mode with a low toughness.

In contrast, as mentioned before, Ma *et al.* [19] have shown that silane modified CNTs dispersed homogeneously in epoxy and resulted in improved interfacial adhesion between nanotubes and epoxy matrix and a moderate increase in K_{IC}. Gersappe [52] also found that as the interaction between polymer chains and nanoparticles increased, the work to failure increased. Similarly, Xu *et al.* [53] suggested that a strong interface is needed to improve the toughness in polymer nanocomposites. During stretching, as the polymer chains preferentially align along the stretching direction, the strong interaction of the nano-fillers (clay layers in this case) with matrix helped move them with the polymer chains and they acted as temporary cross-links during deformation. However, contrary to this particle mobility concept, traditional rigid particle toughening is based on the idea of a weak interface between particles and polymer matrix. That is, the particles must debond at the interface and create free volume in the material on a sub-micron level. This changes the stress state in the material surrounding the particles and induces extensive plastic deformation of the matrix through such mechanisms as crazing, shear yielding, etc [54-58].

Liu *et al.* [59], in line with the observations of the current study, found that the strong interfacial adhesion was responsible for significant improvement in elastic modulus due to effective load transfer but reduced elongation-to-break. Similarly, we have recently shown that in polyamide 6/ clay nanocomposites, nucleation occurs at the silicate surface during crystallization of the matrix and crystalline lamellae align normal to the lateral interface (on both sides) of each clay layer and matrix [60]. These preferentially organized layers are around 30-40 nm (including both sides) for each clay layer at 10 wt% of organoclay loading. As the interplatelet distance is smaller, the entire lamellae in the region are highly constrained. Furthermore, due to the strong tethering junctions between individual clay layer and matrix, full-scale debonding at the polymer -clay interface was rarely observed, indicating that the constraint on the polymer adjacent to the clay was not relieved, limiting the ability of the polymer to undergo plastic deformation. Brosse *et al.* [61] in their very recent work on polyamide 6/multi-walled CNT nanocomposites showed

that the polyamide lamellae even grow from the nanotube surfaces and align normal to the latter. This epitaxial growth was attributed to the crystallographic lattice matching between CNTs and polyamide crystals. Preferentially organized lamellae are ~200 nm in length at 0.1 wt% nanotube loading; when the loading was increased to 1 wt%, their length decreased to 60 nm indicating the increased confinement of polyamide chains. Even in polypropylene/CNT [62] and polyethylene/ CNT [63] nanocomposites, strong nucleating action occurred with nanotubes and transcrystalline layers were observed around them. This constraint effect is probably one of the major reasons for the brittle behavior of polymer/CNT nanocomposites.

On the contrary, larger area associated with slow crack growth in the binary blend (P1) consumes greater amount of energy giving rise to higher impact energy. Ductile tearing on adjacent planes is evident and contributes to the energy absorption in this material (Figure 6a). In addition, fine parallel bands (striations) are visible on the entire fracture surface. These striations have been observed in many ductile polymeric materials, including nylon-rubber blends, and are not only formed by the propagation of the main crack, but also associated with secondary cracks, which initiate at separate nuclei and propagate radially outwards [64]. This behavior is also evident in our material (Figure 6b). Based on previous studies on the impact fracture behavior of polymer/ rubber blends [65, 66] and TEM observations of the fracture zone in the current study, it is believed that the striations are formed due to the severe stretching of the voided matrix material after cavitation of the rubber particles. A schematic showing the formation of striations is given in Figure 6c. Due to the similarity in observations with our previous studies and to avoid repetition, TEM micrographs for the binary blend are not shown here but the toughening mechanisms are briefly described below. Toughening started with cavitation of the elastomeric particles because of their low tear-strength. Cavitation was seen even at ~200 μm underneath the fracture surface although there was no indication of any polyamide matrix plastic deformation. Closer to the fracture surface (notch tip), almost all POE-g-MA rubber particles had cavitated followed by stretching of the voided material indicating yielding of the matrix. Near the fracture surface, extremely large stretching in the range of several hundred percent was observed and the particles coalesced to an extent that it is difficult to identify them individually.

It is surprising and interesting to note that the hackles (representing brittle fracture) seen in the binary nanocomposites are completely absent on the notched impact fracture surfaces of ternary nanocomposites. Predominant ductile tearing behavior and parallel striations are found similar to the binary blend. A representative SEM micrograph for polyamide 6/CNT/POE-g-MA at 5 wt% nanotube loading is shown in Figure 7a. It is thought that the presence of two fillers would affect their level of compatibility with the surrounding phase, which can be seen in the deformation features associated with them [32]. However, there is even no evidence of interface debonding of both fillers and pull-out of nanotubes and/or voids that represent the debonded nanotubes. This again ascertains the fact that similar to nanoscale high aspect ratio clay layers, debonding (or pull-out) of individual nanotubes from matrix is difficult especially when strong tethering

junctions exist between the matrix and carbon nanotubes. TEM observations in the sub-surface damage zone have reinforced this fact.

The presence of carbon nanotubes did not restrict the damage processes associated with POE-g-MA particles. At distances >150 μm from notch tip, the extent of POE-g-MA particle cavitation is limited (Figure 7b). Nanotubes are randomly oriented pointing to the absence of any matrix yielding. Moving closer to the notch tip, the number of cavitated POE-g-MA particles increases and some elongations of the cavities and rubber particles are seen (not shown here). Near the notch tip, severe plastic stretching of the voided matrix is observed; while the rubber particles are severely stretched and appear as thin strips. At this location, cavitated particles have collapsed inside the matrix material and it is even hard to distinguish the rubber particles from the matrix (Figures 7c and 7d). Apart from this, the carbon nanotubes are reorientated along the flow of the yielded matrix within this plastically stretched zone which extends ~10 μm from the notch tip. This observation seems to confirm that plastic deformation or 'mobility' of the polymer matrix leads to the 'mobility' of the nano-fillers which, (unlike micron-sized fillers), are able to actively participate in the mechanical response of the matrix polymer under an applied stress field.

4. Summary

Electrically conductive and super-tough (in terms of specific notched impact energy) polyamide-based nanocomposites are developed and their fracture behavior studied. The results show the importance of obtaining the correct and controlled microstructure to improve the functionality of these materials regarding electrical conductivity and toughness. The absence of nanotubes inside the rubber particles and their entire presence in the continuous matrix enhanced the electrical conductivity owing to the volume exclusion effect; while at the same time, the dispersed rubber particles were able to participate in the toughening processes similar to binary polymer/rubber blends increasing the notched impact energy of these materials. These results are very significant particularly when compared to the polymer/rubber blends with micro-sized particles like glass fibers. For example, Paul and co-workers [67, 68] have reported that a huge 45 wt% elastomer phase is required to toughen polyamide 6 having 15 wt% glass fibers.

Acknowledgements

We would like to thank the Australian Research Council (ARC) for the continuous support of this research project on "*Polymer Nanocomposites*". We acknowledge Professor Zhi-Min Dang of the Key Laboratory of the Ministry of Education on Nanomaterials, Beijing University of Chemical Technology, China, for conductivity measurements of the studied materials.

References

[1] Tjong SC. Mater Sci Engng R 2006;53:73-197.

[2] Nosonovsky M, Bhushan B. Mater Sci Engng R 2007;58:162-193.
[3] Baur J, Silverman E. MRS Bull 2007;32:328-334.
[4] Dasari A, Yu Z-Z, Mai Y-W. Mater Sci Engng R 2009;63:31-80.
[5] Xie XL, Mai Y-W, Zhou XP. Mater Sci Engng R 2005;49:89-112.
[6] Thostenson ET, Ren ZF, Chou TW. Compos Sci Technol 2001;61:1899-1912.
[7] Andrews R, Weisenberger MC. Curr. Opin. Solid State Mater Sci 2004;8:31-37.
[8] Fiedler B, Gojny FH, Wichmann MHG, Nolte MCM, Schulte K. Compos Sci Technol 2006;66:3115-3125.
[9] Coleman JN, Khan U, Gun'ko YK. Adv Mater 2006;18:689-706.
[10] Zhang QM, Li H, Poh M, Xia F, Cheng Z-Y, Xu H, Huang C. Nature 2002;419:284-287.
[11] Thostenson ET, Chou TW. Carbon 2006;44:3022-3029.
[12] Koerner H, Liu W, Alexander M, Mirau P, Dowty H, Vaia RA. Polymer 2005;46:4405-4420.
[13] Satapathy BK, Weidisch R, Potschke P, Janke A. Compos Sci Technol 2007;67:867-879.
[14] Trujillo M, Arnal ML, Muller AJ, Laredo E, Bredeau St, Bonduel D, Dubois P. Macromolecules 2007; 40: 6268-6276.
[15] Meincke O, Kaempfer D, Weickmann H, Friedrich C, Vathauer M, Warth H. Polymer 2004; 45:739-748.
[16] Gojny FH, Wichmann MHG, Fiedler B, Schulte K. Compos Sci Technol 2005;65:2300-2313.
[17] Peigney A, Laurent Ch, Flahaut E, Bacsa RR, Rousset A. Carbon 2001;39:507-514.
[18] Gorga RE, Cohen RE. J Appl Polym Sci Part B: Polym Phys 2004;42:2690-2702.
[19] Ma PC, Kim JK, Tang BZ. Compos Sci Technol 2007;67:2965-2972.
[20] Barber AH, Cohen SR, Wagner HD. Appl Phys Lett 2003;82:4140-4142.
[21] Cooper CA, Cohen SR, Barber AH, Wagner HD. Appl Phys Lett 2002;81:3873.
[22] Barber AH, Cohen SR, Eitan A, Schadler LS, Wagner HD. Adv Mater 2006;18:83-87.
[23] Windle AH. Compos Sci Technol 2007;67:929-930.
[24] Wichmann MHG, Schulte K, Wagner HD. Compos Sci Technol 2008;68:329-331.
[25] Gao Y-C, Mai Y-W, Cotterell B. J Appl Math Phys (ZAMP) 1988;39:550-572.
[26] Bhattacharyya AR, Sreekumar TV, Liu T, Kumar S, Ericson LM, Hauge RH, Smalley RE. Polymer 2003;44:2373-2377.
[27] Jia Z, Wang Z, Xu C, Liang J, Wei B, Wu D, Zhu S. Mater Sci Engng A 1999;271:395-400.
[28] Johnsen BB, Kinloch AJ, Mohammed RD, Taylor AC, Sprenger S. Polymer 2007;48:530-541.
[29] He C, Liu T, Tjiu WC, Sue H-J, Yee AF. Macromolecules 2008;41:193-202.
[30] Dasari A, Yu Z-Z, Mai Y-W. In: Nano- and Micromechanics of Polymer Blends and Composites. Karger-Kocsis J, Fakirov S, editors. Munich: Hanser Publishers; 2009. p. 374.
[31] http://www.fibrils.com

[32] Lim S-H, Dasari A, Yu Z-Z, Mai Y-W, Liu S, Yang MS. Compos Sci Technol 2007;67: 2914-2923.
[33] Dasari A, Yu Z-Z, Mai Y-W, Yang MS. J Nanosci Nanotechnol 2008;8:1901-1912.
[34] Dasari A, Yu Z-Z, Mai Y-W. Polymer 2005;46:5986-5991.
[35] Gonzalez I, Eguiazabal JI, Nazabal J. Compos Sci Technol 2006;66:1833-1843.
[36] Khatua BB, Lee DJ, Kim HY, Kim JK. Macromolecules 2004;37:2454-2459.
[37] Dong WF, Zhang XH, Liu YQ, Gui H, Wang QG, Gao JM, Song ZH, Lai JM, Huang F, Qiao JL. Polym Intl 2007;56:870-874.
[38] Asai S, Hayakawa Y, Suzuki K, Sumita M. Kob Ronb 1991; 48: 635-640.
[39] Thongruang W, Balik CM, Spontak RJ. J Polym Sci Part B: Polym Phys 2002;40:1013-1025.
[40] Feng JY, Chan CM. Polym Engng Sci 1998;38:1649-1657.
[41] Bin Y, Xu C, Agari Y, Matsuo M. Colloid Polym Sci 1999; 277: 452-461.
[42] Sandler JKW, Kirk JE, Kinloch IA, Shaffer MSP, Windle AH. Polymer 2003;44:5893-5899.
[43] Bryning MB, Islam MF, Kikkawa JM, Yodh AG. Adv Mater 2005;17:1186-1191.
[44] Bai JB, Allaoui A. *Compos Part A* 2003;34:689-694.
[45] Kim YJ, Shin TS, Choi HD, Kwon JH, Chung YC, Yoon HG. Carbon 2005;43:23-30.
[46] Allaoui A, Bai S, Cheng HM, Bai JB. Compos Sci Technol 2002;62:1993-1998.
[47] Li J, Ma PC, Chow WS, To CK, Tang BZ, Kim JK. Adv Funct Mater 2007;17:3207-3215.
[48] Potschke P, Fornes TD, Paul DR. Polymer 2002;43:3247-3255.
[49] Shaffer MSP, Windle AH. Adv Mater 1999;11:937-941.
[50] Sandler J, Shaffer MSP, Prasse T, Bauhofer W, Schulte K, Windle AH. Polymer 1999;40: 5967-5971.
[51] Potschke P, Bhattacharyya AR, Janke A, Goering H. Compos Interf 2003;10:389-404.
[52] Gersappe D. Phys Rev Lett 2002; 89: 058301.
[53] Xu W, Raychowdhury S, Jiang DD, Retsos H, Giannelis EP. Small 2008; 4: 662-669.
[54] Thio YS, Argon AS, Cohen RE. Polymer 2004;45:3139-3147.
[55] Thio YS, Argon AS, Cohen RE, Weinberg M. Polymer 2002;43:3661-3674.
[56] Zuiderduin WCJ, Westzaan C, Huetink J, Gaymans RJ. Polymer 2003;44:261-275.
[57] Bartczak Z, Argon AS, Cohen RE, Weinberg M. Polymer 1999;40:2347-2365.
[58] Lazzeri A, Zebarjad SM, Pracella M, Cavalier K, Rosa R. Polymer 2005;46:827-844.
[59] Liu T, Tong Y, Zhang WD. Compos Sci Technol 2007;67:406-412.
[60] Dasari A, Yu Z-Z, Mai Y-W. Macromolecules 2007;40:123-130.
[61] Brosse AC, Girault ST, Piccione PM, Leibler L. Polymer 2008;49:4680-4686.
[62] Miltner HE, Grossiord N, Lu K, Loos J, Koning CE, van Mele B. Macromolecules 2008;41: 5753-5762.
[63] Haggenmueller R, Fischer JE, Winey KI. Macromolecules 2006;39:2964-2971.
[64] Muratoglu OK, Argon AS, Cohen RE, Weinberg M. Polymer 1995;36:4771-4786.
[65] Bartczak Z, Argon AS, Cohen RE, Weinberg M. Polymer 1999;40;2331-2346.

[66] van der Wal A, Gaymans RJ. Polymer 1999;40:6067-6075.
[67] Cho JW, Paul DR. J Appl Polym Sci 2001;80:484-497.
[68] Laura DM, Keskkula H, Barlow JW, Paul DR. Polymer 2003;44:3347-3361.

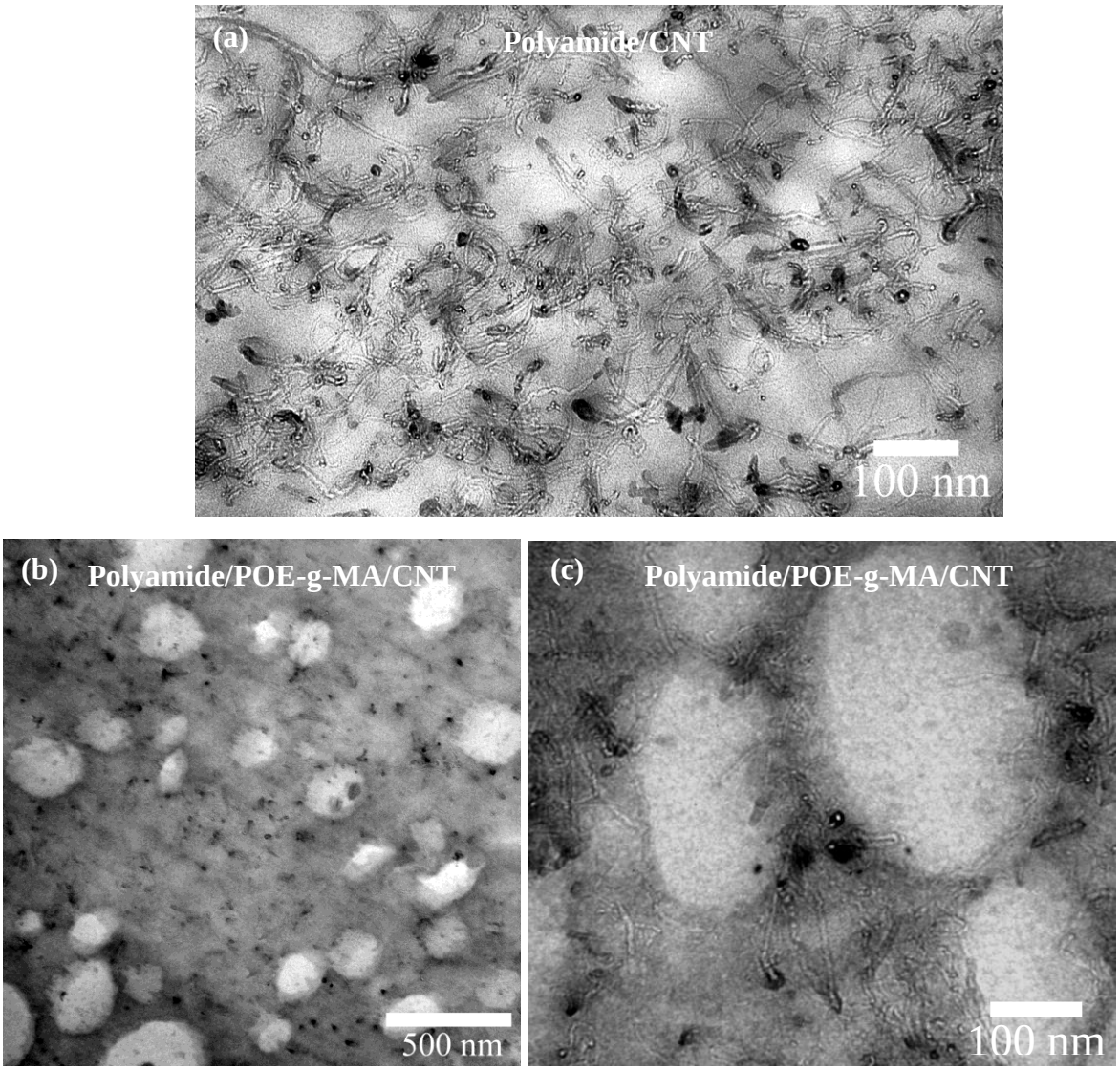

Figure 1. TEM micrographs showing the dispersion quality of carbon nanotubes (5 wt%) in (a) polyamide 6 matrix; and (b, c) polyamide 6 with 20 wt% of POE-g-MA. In (b) and (c), due to the negative staining, POE-g-MA particles appear lighter than polyamide matrix.

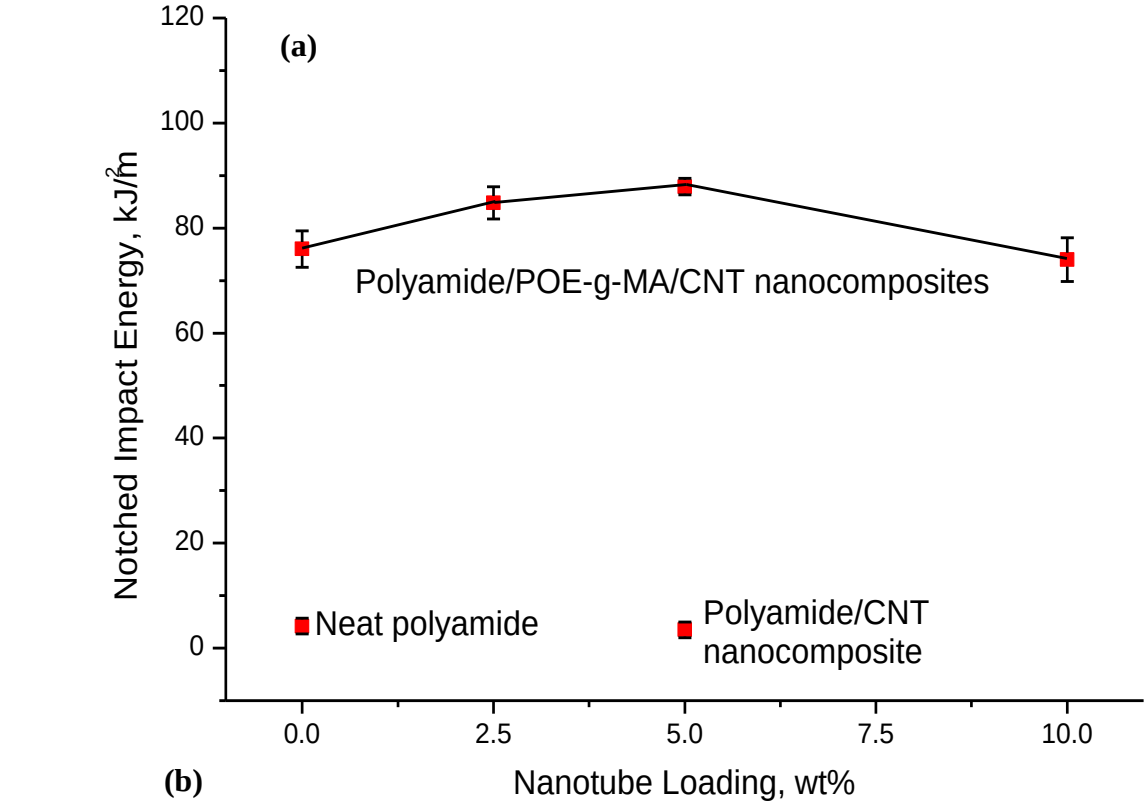
(a)
Notched Impact Energy, kJ/m2
120
100
80
60
40
20
0
Polyamide/POE-g-MA/CNT nanocomposites
Neat polyamide
Polyamide/CNT nanocomposite
0.0
2.5
5.0
7.5
10.0
Nanotube Loading, wt%

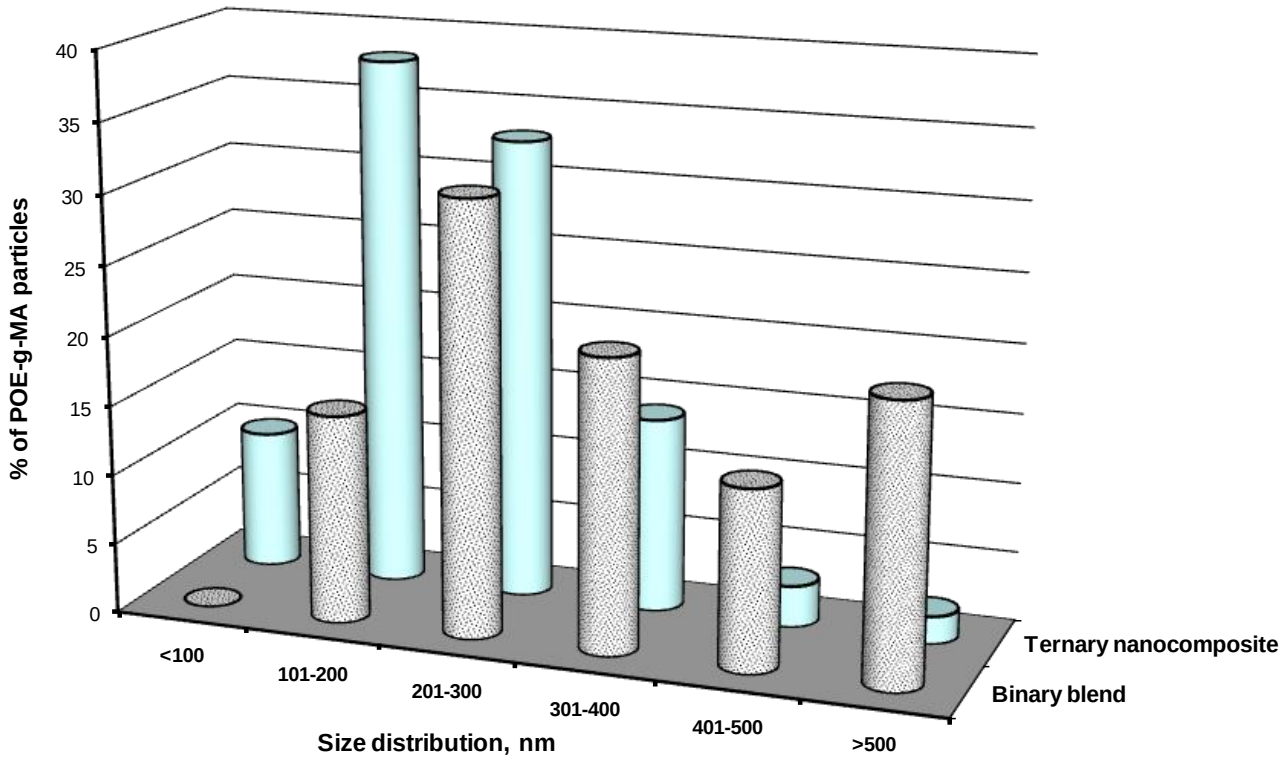
(b)
% of POE-g-MA particles
40
35
30
25
20
15
10
5
0
<100
101-200
201-300
301-400
401-500
>500
Size distribution, nm
Ternary nanocomposite
Binary blend

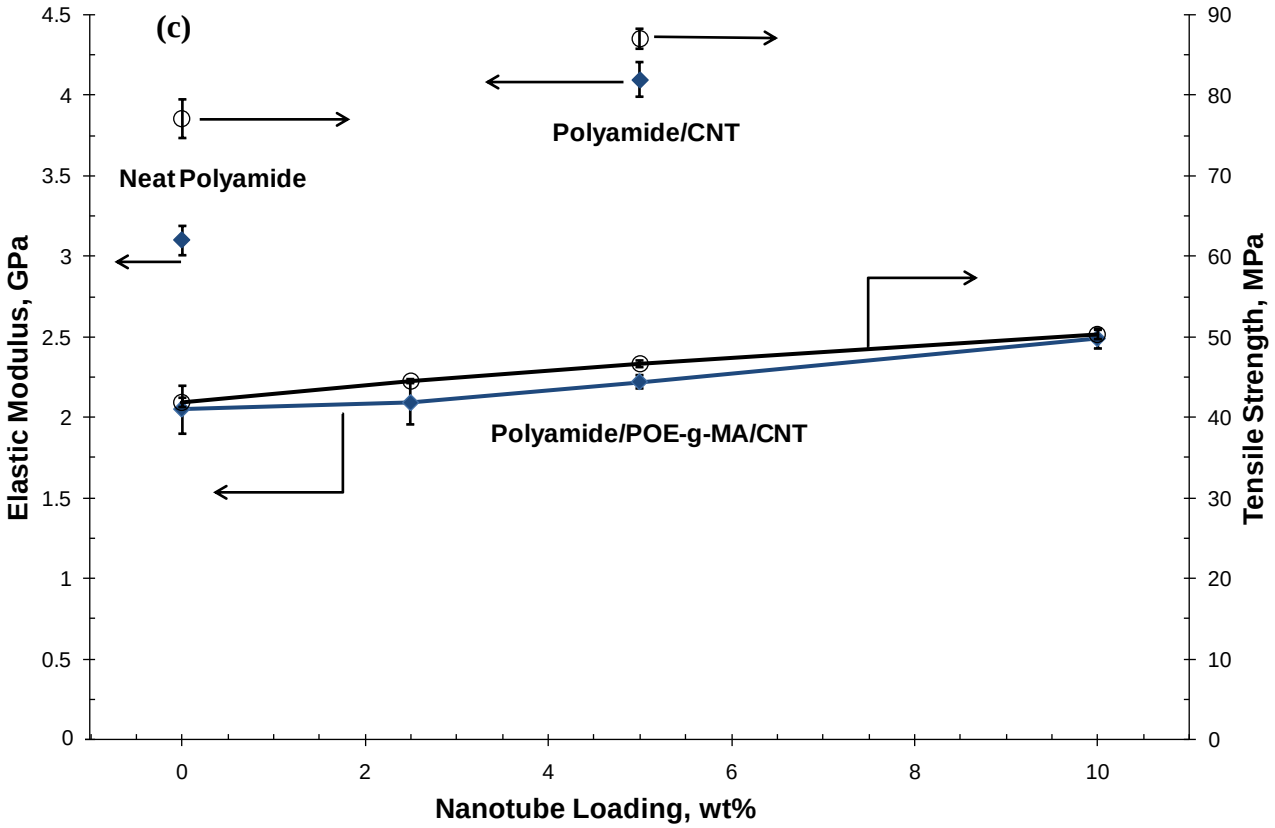

Figure 2. (a) Notched Izod impact energy of polyamide 6/POE-g-MA blends with varying nanotube loading; (b) POE-g-MA particle size distributions in polyamide 6/POE-g-MA binary blend and polyamide 6/POE-g-MA/CNT ternary nanocomposite at 5 wt% nanotube; and (c) elastic modulus and tensile strength values for polyamide 6/POE-g-MA blends with varying nanotube loading. Data for neat polyamide 6 and polyamide 6 with 5 wt% CNT binary nanocomposite is provided in (a) and (c) for comparison. POE-g-MA loading is fixed at 20 wt% in both binary and ternary materials.

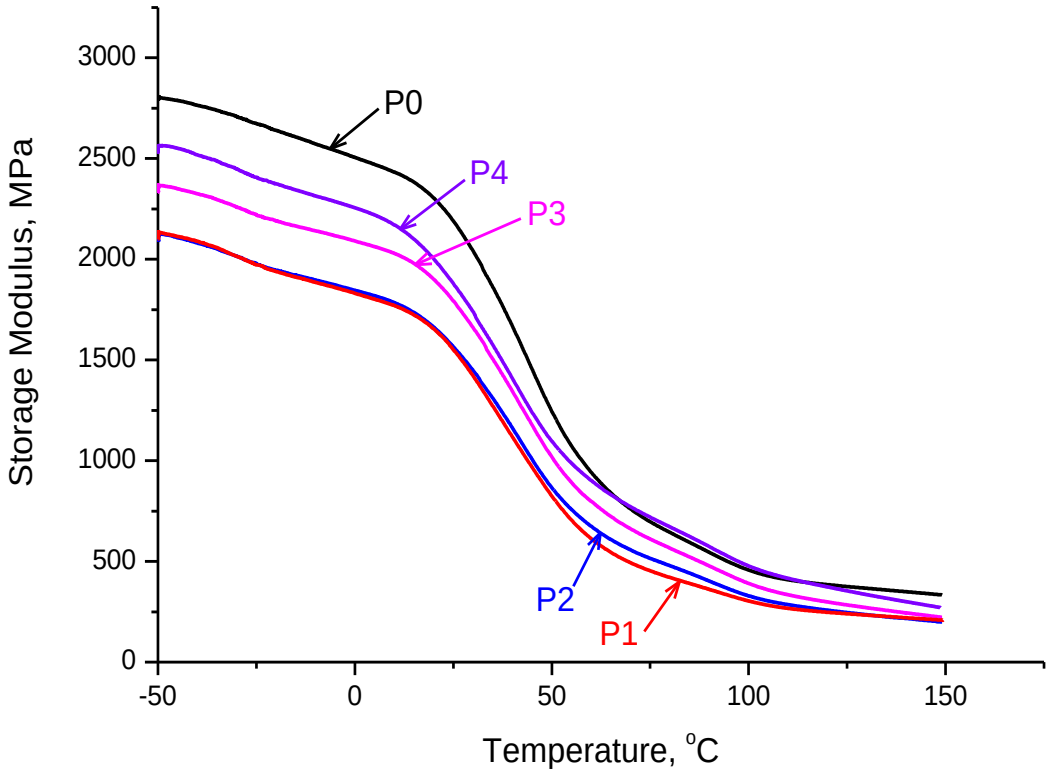

Figure 3. Storage modulus *versus* temperature for neat polyamide 6 (P0), polyamide 6/POE-g-MA blend (80/20 - P1), and polyamide 6/POE-g-MA/CNT ternary nanocomposites with different nanotube loading (77.5/20/2.5 - P2, 75/20/5 - P3, 70/20/10 - P4).

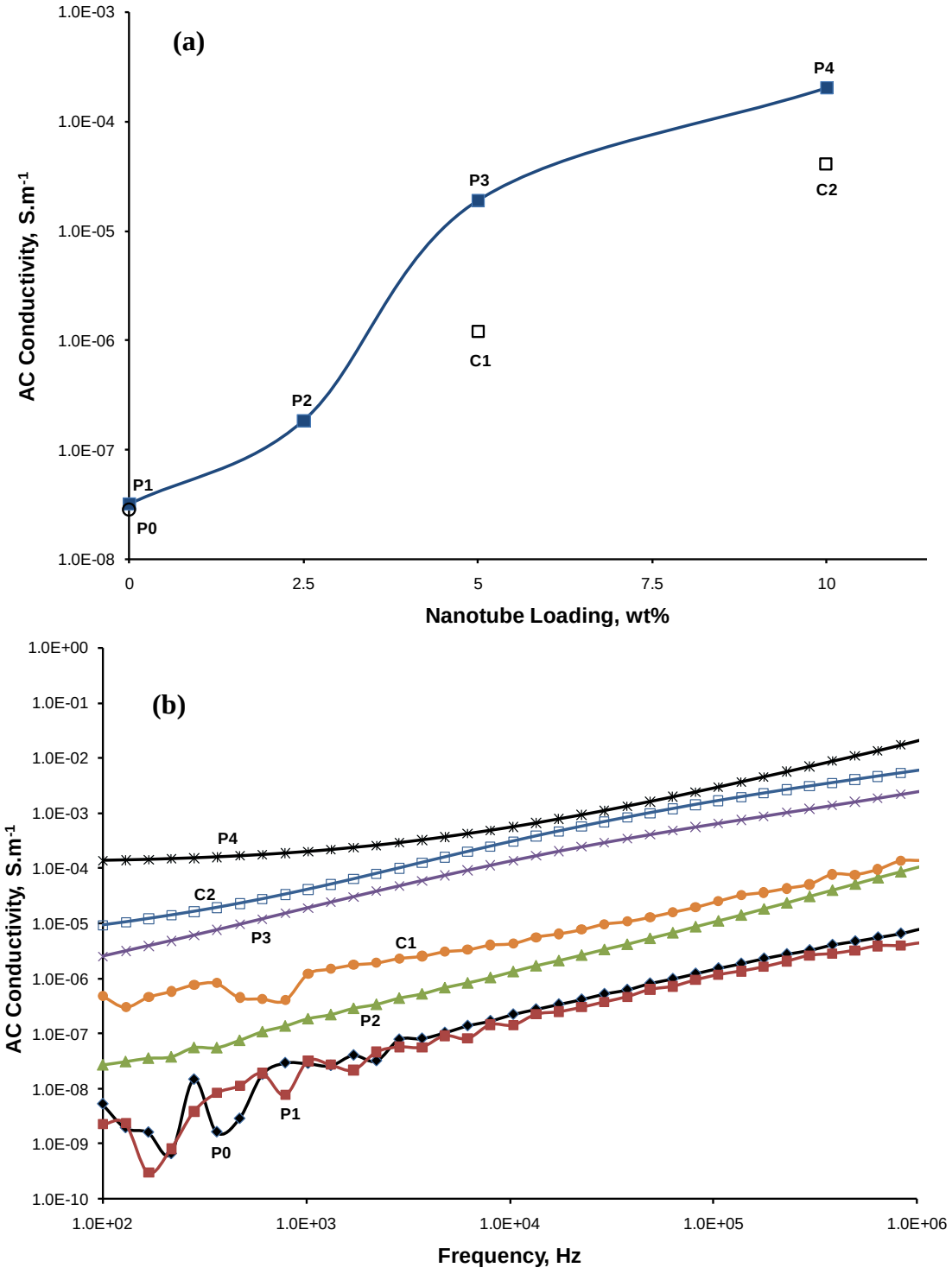

Figure 4. (a) Effect of nanotube loading at a frequency of 10^3 Hz; and (b) frequency dependence on AC electrical conductivities of polyamide 6/POE-g-MA materials (P1 to P4). Data for neat polyamide 6 (P0) and binary polyamide 6/CNT nanocomposites at 5 (C1) and 10 (C2) wt% CNT are also shown for comparison purpose.

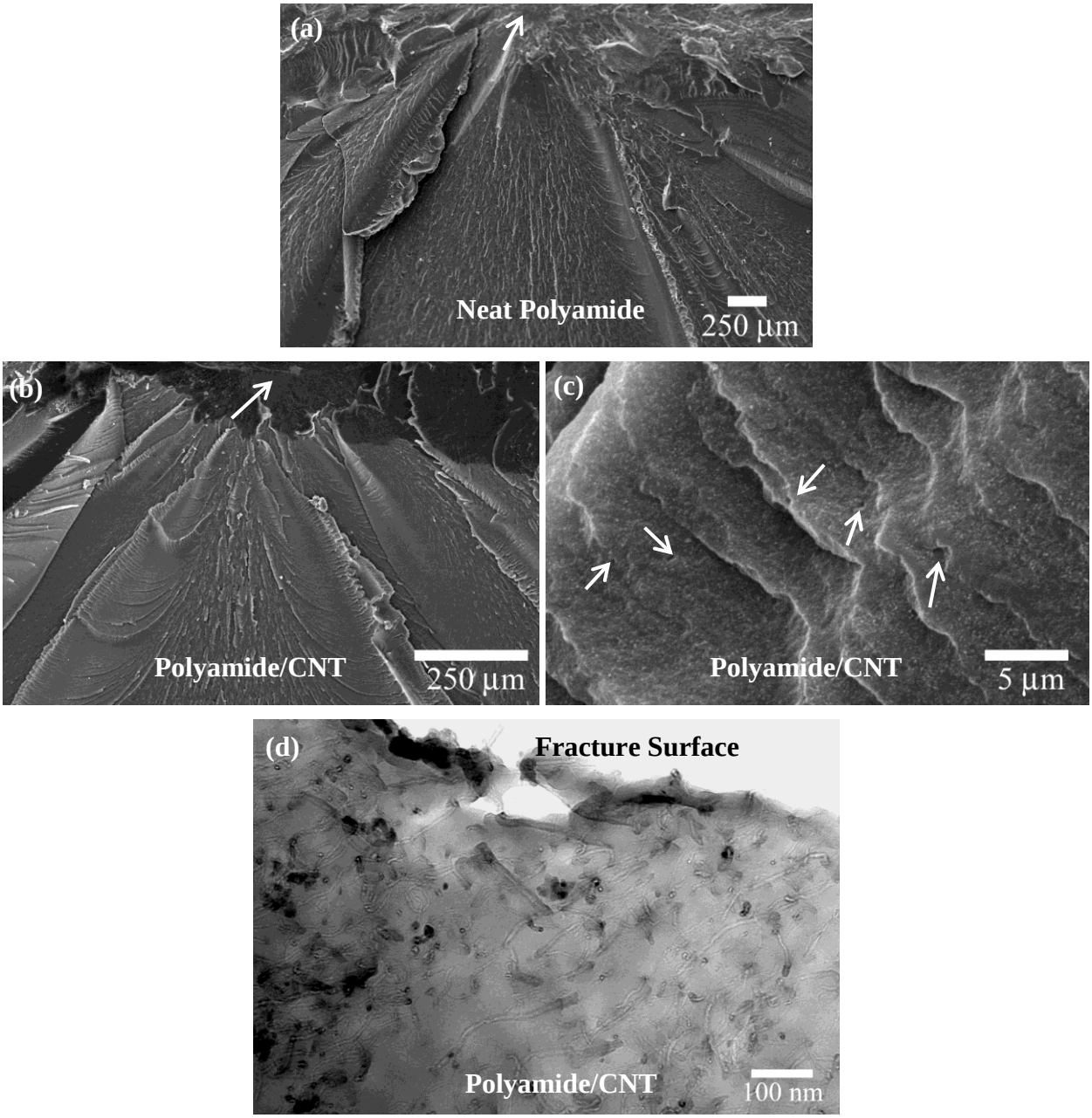

Figure 5. Low (a, b) and high (c) magnification SEM micrographs of impact fracture surfaces of (a) neat polyamide 6 and (b, c) binary polyamide 6/CNT nanocomposite with 5 wt% nanotube; arrows in (a, b) indicate the primary crack initiation site and in (c) point to the voids that may be formed due to the removal of small pieces of material during the fast fracture process. (d) TEM micrograph taken within the sub-critically deformed zone for binary polyamide with 5 wt% CNT nanocomposite suggesting the absence of any deformation feature associated with nanotubes (even at the fracture surface) apart from their slight orientation along the matrix plastic flow direction.

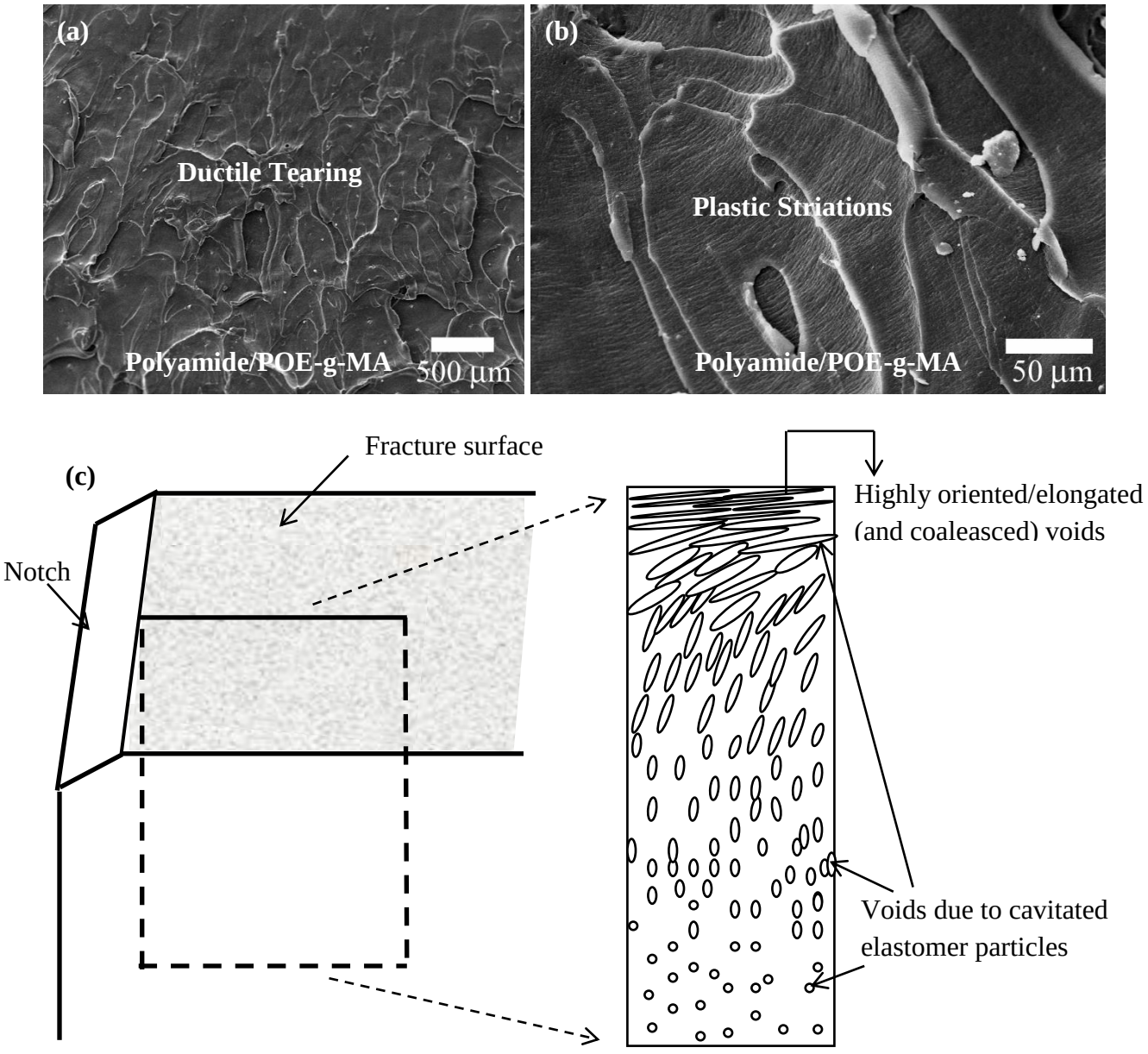

Figure 6. Low (a) and high (b) magnification SEM micrographs of the impact fracture surface of polyamide/POE-g-MA binary blend showing (a) ductile tearing marks and (b) plastic striations; (c) schematic showing a typical fracture zone (in a plane perpendicular to the fracture surface and parallel to the crack propagation direction) in a polymer/rubber blend. Strain varies with distance from the crack and is reflected in the orientation/elongation of the cavities. Round voids can be seen in the regions far away from the fracture surface; the voids increase in size with their position nearer the fracture surface and have a more elongated shape. The direction of elongation of these voids is in the crack propagation direction. These elongated voids are formed as a result of the strong plastic deformation of the surrounding matrix. Near the fracture surface, where the strain direction is

parallel to the fracture surface, extensive stretching of cavitated particles in the range of several hundred percent occurs along with particle coalescence giving the appearance of thin strips. When viewed normal to this direction (that is, on the fracture surface), they appear as striations.

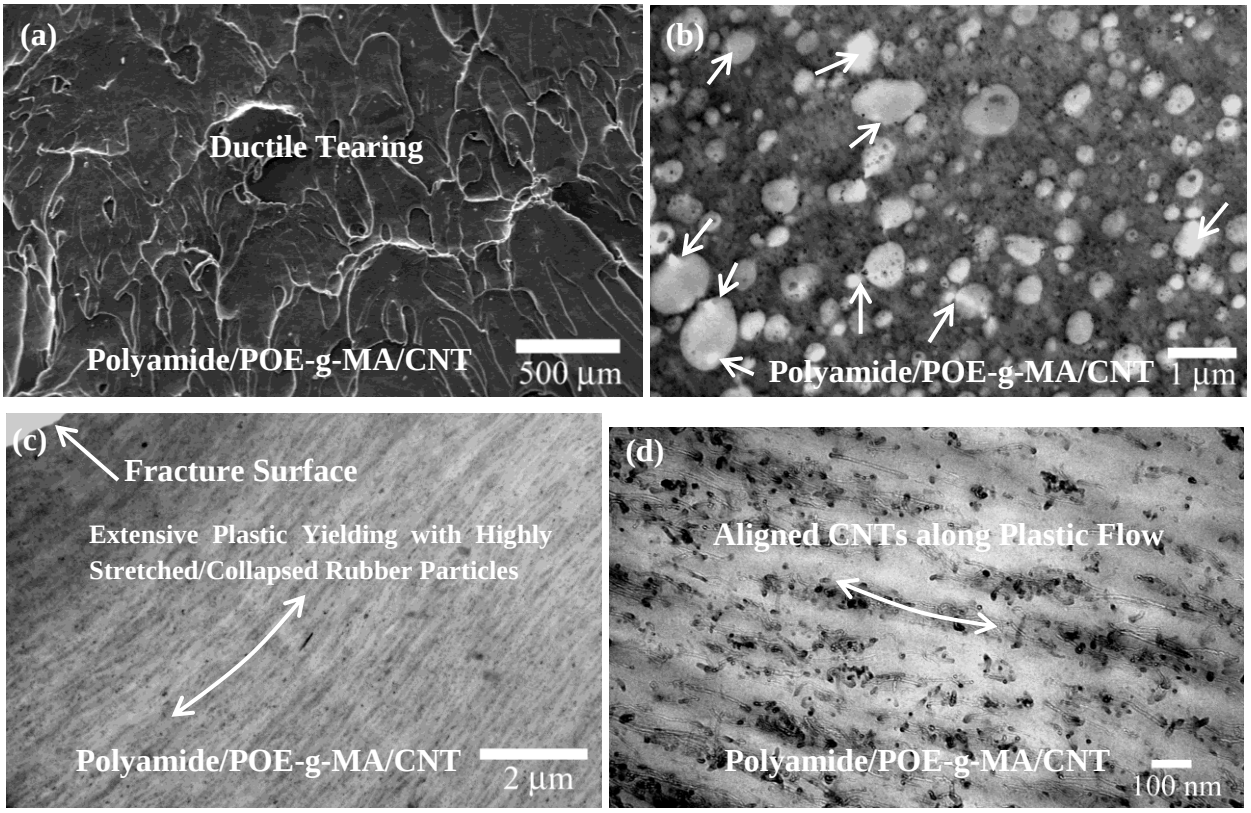

Figure 7. (a) SEM micrograph of impact fracture surface of polyamide/POE-g-MA/CNT ternary nanocomposite having 20 wt% POE-g-MA and 5 wt% CNT showing ductile tearing marks. (b-d) Series of TEM micrographs taken within the sub-critically deformed zone for the same material showing (b) some cavitation of rubber particles at ~100 μm beneath the fracture surface; (c, d) extensive plastic flow near the fracture surface with highly stretched and collapsed rubber particles along with alignment and reorientation of nanotubes along the plastic flow.